M. Martín-Neira
Radio-Frequency Systems Division, ESTEC, Noordwijk, The Netherlands

A Passive Reflectometry and Interferometry System (PARIS): Application to Ocean Altimetry

Abstract To date, altimetry from space has mainly been limited to nadir-looking-type instruments because of the difficulty of realising a precise wide-swath radar altimeter. A concept is presented that can be used to perform altimetry measurements over points along directions other than nadir, by making use of a passive instrument. The method is applied here to ocean altimetry in particular.

This concept, based on the existence of sources of opportunity, consists of combining the direct signal and the signal that is reflected by the Earth's surface to obtain the desired measurement. It can be regarded as a multistatic radar for which the transmitters and the receivers belong to different systems. Because of the combination of direct and reflected signals, this concept has been called the 'Passive Reflectometry and Interferometric System' (PARIS).

1. Introduction

As was recognised during the Consultative Meeting on Imaging Altimeter Requirements and Techniques held in June 1990 at Mullard Space Science Laboratory (UK), the ability to carry out high-precision ocean altimetry over a swath with high spatial resolution would revolutionise many fields of Earth science: *'Some form of multi-beam altimetry would offer the possibility of achieving satisfactory sampling of the ocean mesoscale flows, and would, in addition, improve the ability to study other spatially and temporally variable oceanographic phenomena such as wave and wind fields, and ocean sea-ice interactions'* (see Ref. 1). The PARIS concept is directed towards such a multi-beam altimetry objective.

A number of systems were identified as possible candidates for the different scientific purposes, and the main parameters relating to the performance of each system – namely vertical precision, spatial resolution and swath – have been studied. The different types of systems that were considered and their associated performances are presented in Table 1, the constellation of n pulse-limited altimeters being the one recommended by the study team for ocean applications and some specific land/ice studies[1].

A new concept for ocean altimetry is presented which consists basically of taking signals of opportunity, which are reflected by the ocean surface, and combining them with the direct path signal, in order to provide an estimate of the ocean's height over the geoid[4]. There are two major aspects to PARIS: the first is that the altimetry is performed in a bistatic configuration and therefore at points off-nadir; and the second is the use of signals of opportunity. Bistatic altimetry is still pulse-limited, and could save half the number of satellites in the recommended n-satellite pulse-limited constellation without narrowing the swath[1,2].

The study presented here describes the PARIS concept from system geometry up to instrument configuration. A preliminary analysis is given with the intention of presenting the overall concept, leaving aside some of the more detailed points that still require further study. A numerical example used to illustrate the analysis relies on the satellites of the Global Positioning System (GPS) as sources of opportunity[3]. Altimetry is performed along about five subtracks each 15 km wide, which would be spread over a swath of 1000 km. Because of the limited bandwidth of the GPS signals, the height accuracy performance obtained is only 0.7 m. If opportunity signals were available with bandwidths of a few hundred MHz, centimetre-level accuracy would also be feasible.

Table 1. Likely instrument performance characteristics

Instrument	Vert. precision (m)	Spatial resolution (m)	Swath (km)
Across-track-scanning phased-array altimeter	5	300	100
Interferometric side-looking radar altimeter with synthetic aperture	3	30	100
Small-dish interferometric altimeter	0.1	10 k	50
Single pulse-limited altimeter	0.1	10 k	—
Constellation of n pulse-limited altimeters	0.02	10 k	—
Pencil-beam beam-limited altimeter	1	500	5

2. Specular reflection point computation

In this section the coordinates of the point of specular reflection are computed for the geometry of the system shown in Figure 1, assuming a spherical Earth.

Let xy be the plane containing transmitter, receiver and reflection point, $T(x_t,y_t)$ the transmitter point, $R(x_r,y_r)$ the receiver point, $P(x,y)$ the point of specular reflection, ϕ the angular polar coordinate of P and r the radius of the Earth. Let $x'y'$ be a system of coordinates that is obtained by rotating the xy coordinates and angle ϕ counterclockwise and then translating it along the new $+x$-axis a distance equal to

the radius of the sphere r. Then we have the following relationship between xy and $x'y'$:

$$\begin{bmatrix} x' \\ y' \end{bmatrix} = \begin{bmatrix} \cos\phi & \sin\phi \\ -\sin\phi & \cos\phi \end{bmatrix} \begin{bmatrix} x \\ y \end{bmatrix} - \begin{bmatrix} r \\ 0 \end{bmatrix} \tag{1}$$

We first transform the transmitter and receiver coordinates to the $x'y'$ system

$$\begin{bmatrix} x_t' \\ y_t' \end{bmatrix} = \begin{bmatrix} \cos\phi & \sin\phi \\ -\sin\phi & \cos\phi \end{bmatrix} \begin{bmatrix} x_t \\ y_t \end{bmatrix} - \begin{bmatrix} r \\ 0 \end{bmatrix} \tag{2}$$

$$\begin{bmatrix} x_r' \\ y_r' \end{bmatrix} = \begin{bmatrix} \cos\phi & \sin\phi \\ -\sin\phi & \cos\phi \end{bmatrix} \begin{bmatrix} x_r \\ y_r \end{bmatrix} - \begin{bmatrix} r \\ 0 \end{bmatrix} \tag{3}$$

because in this $x'y'$ system the condition for specular reflection (Snell's law) can be easily expressed as

$$\frac{x_t'}{y_t'} = -\frac{x_r'}{y_r'} \tag{4}$$

Substituting Equations 2 and 3 into Equation 4 gives

$$\frac{x_t\cos\phi + y_t\sin\phi - r}{-x_t\sin\phi + y_t\cos\phi} = -\frac{x_r\cos\phi + y_r\sin\phi - r}{-x_r\sin\phi + y_r\cos\phi} \tag{5}$$

and operating this expression one obtains

$$2(x_tx_r - y_ty_r)\sin\phi\cos\phi - (x_ty_r + y_tx_r)(\cos^2\phi - \sin^2\phi) -$$

$$r\sin\phi(x_t + x_r) + r\cos\phi(y_t + y_r) = 0 \tag{6}$$

Making the following change of variable

$$t = \tan\frac{\phi}{2} \tag{7}$$

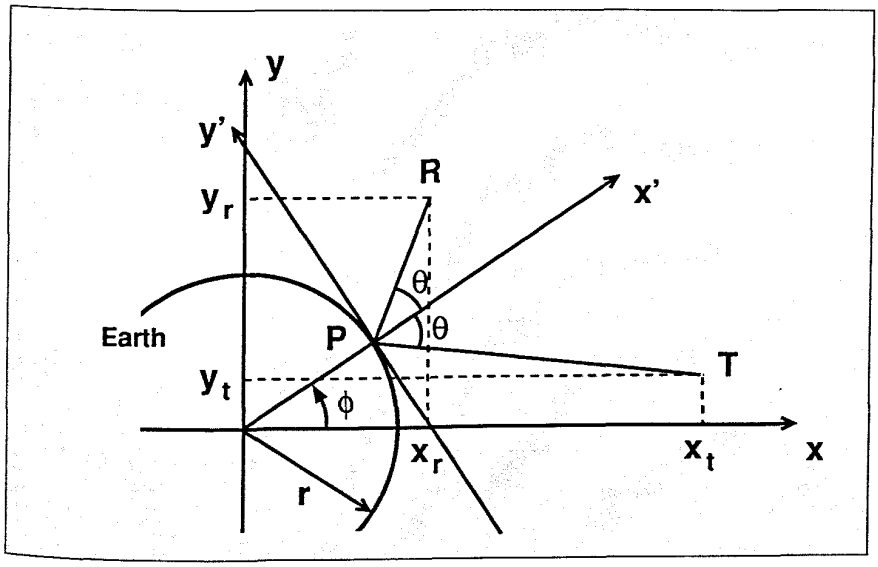

Figure 1. System geometry for computation of the coordinates of the specular reflection point

Equation 6 becomes

$$2(x_t x_r - y_t y_r)\,\frac{2t}{1+t^2}\,\frac{1-t^2}{1+t^2} - (x_t y_r + y_t x_r)\left[\left(\frac{1-t^2}{1+t^2}\right)^2 - \left(\frac{2t}{1+t^2}\right)^2\right] -$$

$$r\,\frac{2t}{1+t^2}\,(x_t + x_r) + r\,\frac{1-t^2}{1+t^2}\,(y_t + y_r) = 0 \tag{8}$$

and arranging this expression, the equation of the specular point can finally be written as (spherical mirror equation)

$$c_4 t^4 + c_3 t^3 + c_2 t^2 + c_1 t + c_0 = 0 \tag{9}$$

where

$$t = \tan\frac{\phi}{2} \tag{10}$$

$$c_0 = (x_t y_r + y_t x_r) - r(y_t + y_r) \tag{11}$$

$$c_1 = -4(x_t x_r - y_t y_r) + 2r(x_t + x_r) \tag{12}$$

$$c_2 = -6(x_t y_r + y_t x_r) \tag{13}$$

$$c_3 = 4(x_t x_r - y_t y_r) + 2r(x_t + x_r) \tag{14}$$

$$c_4 = (x_t y_r + y_t x_r) + r(y_t + y_r) \tag{15}$$

We now proceed to calculate the distance from the receiver to the point of specular reflection as a function of the elevation of the transmitter above the local horizon. For doing this and without loss of generality, we shall assume the receiver to be located along the y-axis at an altitude of h metres over the Earth's surface, so that its coordinates are

$$x_r = 0; \qquad y_r = r + h \tag{16}$$

The coordinates of the transmitter $T(x_t, y_t)$ can be expressed in terms of the elevation angle β above the local horizon plane at the receiver location using the following relations, as directly derived from Figure 2:

$$x_t = r_t \cos(\beta+\gamma);\; y_t = r_t \sin(\beta+\gamma);\; \frac{\sin\left(\frac{\pi}{2} + \beta\right)}{r_t} = \frac{\sin\gamma}{r+h} \tag{17}$$

where r_t is the orbital radius of the transmitter. Manipulating the previous expressions, one obtains

$$x_t = r_t \cos\beta \sqrt{1 - \frac{(r+h)^2}{r_t^2}\cos^2\beta} - (r+h)\sin\beta\cos\beta \tag{18}$$

$$y_t = r_t \sin\beta \sqrt{1 - \frac{(r+h)^2}{r_t^2}\cos^2\beta} + (r+h)\cos^2\beta \tag{19}$$

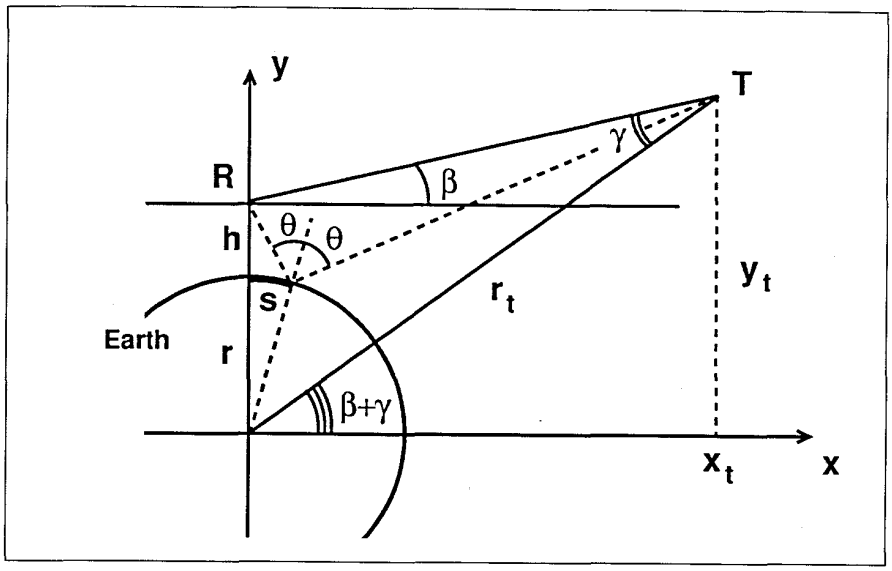

Figure 2. Geometry used to express transmitter coordinates in terms of its elevation angle (β) above the local horizon plane at the receiver location

2.1. Numerical example: GPS transmitters

The quantities that will be computed are the distance from the receiver to the specular reflection point R_2

$$R_2 = \overline{RP} \tag{20}$$

and the arc length s from the subreceiver point to the specular reflection point

$$s = \left(\frac{\pi}{2} - \phi\right) r \tag{21}$$

as a function of the elevation β of the transmitter over the local horizon at the receiver location, as indicated in Figure 2.

In the case where the transmitters are the GPS satellites, we have

$$r_t = 26.5 \times 10^6 \text{ m} \tag{22}$$

and we take the Earth's radius r=6370 km.

Three scenarios have been considered regarding the receiver: a spacecraft at 700 km, an aircraft at 10 km and an aircraft at 1 km altitude. Using the previous equations and values, we obtain the following results:

— Spacecraft at h=700 km altitude:

Elevation β (deg)	Arc length s (km)	Distance R_2 (km)
0	1551	1774
10	1206	1449
20	936	1209
30	726	1036
40	557	913
50	418	827
60	299	768
70	193	729
80	95	707
90	0	700

— Aircraft at $h = 10$ km altitude:

Elevation β (deg)	Arc length s (km)	Distance R_2 (km)
0	204.8	205.2
10	52.6	53.6
20	26.9	28.7
30	17.1	19.8
40	11.8	15.5
50	8.3	13.0
60	5.7	11.5
70	3.6	10.6
80	1.7	10.1
90	0.0	10.0

— Aircraft at $h = 1$ km altitude:

Elevation β (deg)	Arc length s (km)	Distance R_2 (km)
0	65.052	65.064
10	5.628	5.716
20	2.746	2.923
30	1.732	2.000
40	1.197	1.560
50	0.844	1.309
60	0.577	1.155
70	0.365	1.064
80	0.182	1.016
90	0.000	1.000

From these tables, it can be concluded that the specular reflection points corresponding to GPS satellites at elevations greater than about 40° over the local receiver horizon are within a cone with vertex at the receiver point, with a half angle of about 45°, and with its axis aligned along the receiver nadir direction.

2.2. Iso-line computation

In this Section the lines of constant range and constant Doppler for the system are studied. Exact equations are only derived for the constant-range lines when the transmitter is at the zenith of the receiver. In any other case, only a qualitative result for the iso-range lines is presented. In the case of the lines of constant Doppler, very reasonably approximated results are shown.

Iso-range lines

The iso-range lines are defined as those points for which the relative delay between the direct signal and the reflected signal is the same. This condition can be written, with reference to Figure 3, as

$$\overline{TP} + \overline{PR} - \overline{TR} = K \tag{23}$$

where T is the transmitter point, R the receiver point, and P a point on the Earth's surface for which the path difference is K metres.

We assume that the positions of the transmitter and the receiver are known from the navigation information provided by the transmitted signals themselves and that

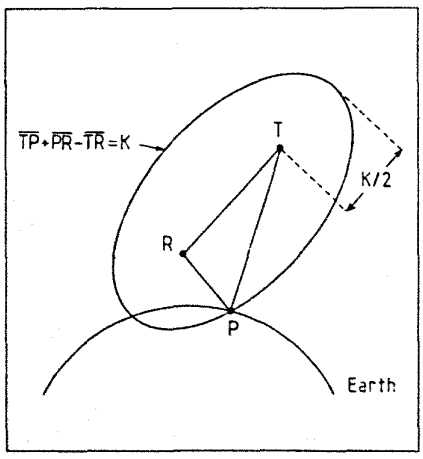

Figure 3. Geometric locus of constant delay between direct and reflected paths

therefore the distance $\overline{TR}$ is a known constant in Equation 23. For this reason, we may write the following equivalent expression for the iso-range lines:

$$\overline{TP} + \overline{PR} = k \tag{24}$$

with k being a constant equal to

$$k = K + \overline{TR} \tag{25}$$

Equation 24 is the equation of an ellipsoid of revolution with foci at the transmitter point T and at the receiver point R as depicted in Figure 3. The intersection of this ellipsoid and the surface of the Earth defines a particular iso-range line. The family of iso-range lines is generated when k is allowed to take different values.

The instrument measures the quantity k and the range processor uses several values of this delay separated by one code chip to perform range discrimination. In order to find the width of the strip on ground defined by two iso-range lines one code chip apart, we have to know the gradient of k as a function of the point P; that is

$$k_s \equiv \frac{1}{\nabla k} = \frac{ds}{dk} \tag{26}$$

where k_s is the spatial sensitivity of the instrument and s is the coordinate measured along a coordinate line perpendicular to the iso-range lines.

In general, the intersection of the ellipsoid defined by Equation 24 and the Earth's surface (modelled also as an ellipsoid of revolution) gives a curve which is not flat. We start the analysis by considering the general case where the transmitter is in any arbitrary direction, but later we will constrain the study to the particular case in which the transmitter is in the zenith direction of the receiver. For this particular configuration, we will calculate the iso-range lines and the spatial sensitivity of the instrument. The conclusions that are applicable to the general case will be pointed out. The Earth will always be approximated by a sphere.

The general case is shown in Figure 4. For the coordinates, we choose an Earth-centred coordinate system such that the receiver is in the x-axis and the transmitter is in the xy plane, so that

$$T = (x_t, y_t, 0); \quad R = (x_r, 0, 0); \quad P = (x, y, z) \tag{27}$$

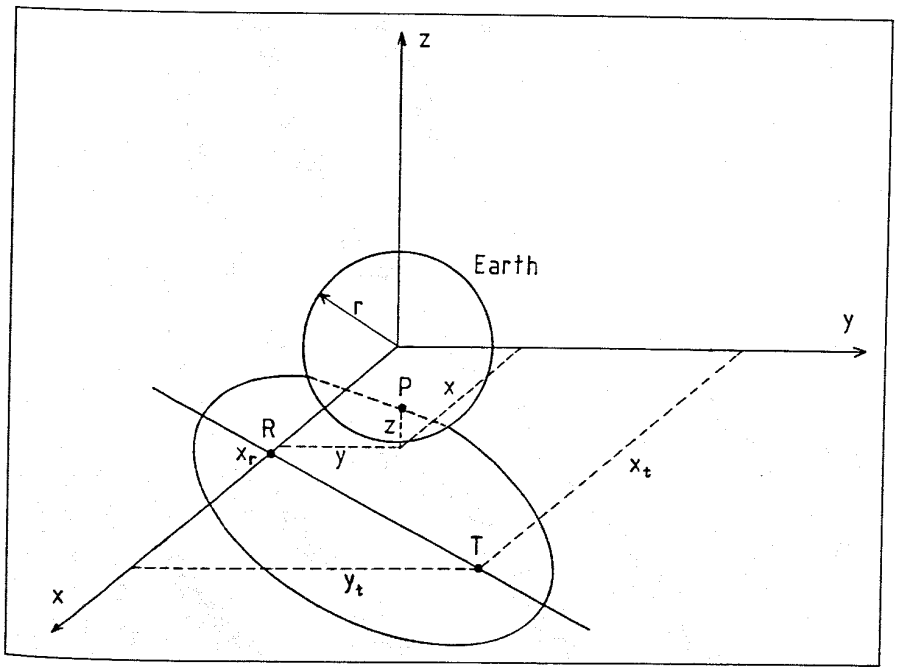

Figure 4. General geometry for the determination of the iso-range lines on the Earth's surface as the intersection of the constant-delay locus and the Earth's sphere

Then, the ellipsoid defined by Equation 24 can be written as

$$\lambda(x-x_t)^2 + (y-y_t)^2 + z^2 + \lambda(x-x_r)^2 + y^2 + z^2 = k \tag{28}$$

and the equation of the Earth's sphere as

$$x^2 + y^2 + z^2 = r^2 \tag{29}$$

The iso-range lines are defined by the intersection of the ellipsoids and the Earth's sphere. When this intersection is calculated, the following equation is found for the projection of the iso-range lines onto the xy plane:

$$ax^2 + by^2 + cxy + dx + ey + f = 0 \tag{30}$$

where the coefficients are given by

$$a = 4(x_t-x_r)^2 \tag{31}$$

$$b = 4y_t^2 \tag{32}$$

$$c = 8(x_t-x_r)y_t \tag{33}$$

$$d = -4(x_t^2+y_t^2-x_r^2)(x_t-x_r) + 4k^2(x_t+x_r) \tag{34}$$

$$e = -4(x_t^2+y_t^2-x_r^2)y_t + 4k^2 y_t \tag{35}$$

$$f = (x_t^2+y_t^2-x_r^2)^2 - 2k^2(2r^2+x_t^2+y_t^2+x_r^2) + k^4 \tag{36}$$

At this point we restrict the analysis to the case when the transmitter is in the zenith direction of the receiver, i.e. when $y_t=0$. In this case, the projection of the iso-range lines onto the xy plane can be written as

$$Ax^2 + Bx + C = 0 \tag{37}$$

with

$$A = 4(x_t-x_r)^2 \tag{38}$$

$$B = -4(x_t+x_r)[(x_t-x_r)^2 - k^2] \tag{39}$$

$$C = (x_t+x_r)^2(x_t-x_r)^2 - 2k^2(2r^2+x_t^2+x_r^2) + k^4 \tag{40}$$

The projections of the iso-range lines onto the xy plane are then given by

$$x = \frac{-B \pm \sqrt{B^2-4AC}}{2A} \tag{41}$$

which are lines parallel to the y-axis. It can be shown by considering the values of x and k at the sub-receiver point that only the positive sign of the square root gives the correct solution. Taking this into account, the equations of the iso-range lines are finally obtained as

$$y^2 + z^2 = r^2 - x^2(k) \tag{42}$$

with

$$x(k) = \frac{(x_t+x_r)[(x_t-x_r)^2 - k^2] + 2k\sqrt{x_tx_rk^2-(x_t-x_r)^2(x_tx_r-r^2)}}{2(x_t-x_r)^2} \tag{43}$$

The iso-range lines are thus circles parallel to the yz-plane and centred about the x-axis, as depicted in case (a) of Figure 5. The range of values of k expands from a minimum value at the sub-receiver point to a maximum value at the point of tangency to the Earth's sphere from the receiver point. These two limits, which are easily derived, are

$$(x_t - x_r) + 2(x_r - r) \leq k \leq \sqrt{x_t^2 + r^2\left(1 - 2\frac{x_t}{x_r}\right)} + \sqrt{x_r^2 - r^2} \tag{44}$$

Now we compute the spatial sensitivity of the instrument. For that we first write Equations 37–40 in the form

$$k^4 - 2Dk^2 + E = 0 \tag{45}$$

with

$$D = (x_t - x)^2 + (x_r - x)^2 + 2(r+x)(r-x) \tag{46}$$

$$E = [(x_t - x)^2 - (x_r - x)^2]^2 \tag{47}$$

In this form, we can calculate the value of k as a function of the x-coordinate by solving Equation 45:

$$k^2 = D \pm \sqrt{D^2 - E} \tag{48}$$

Making the same considerations about the sign of the square root as in the derivation of the iso-range lines, we find that only the positive sign gives the right solution. Thus, after some manipulations, we obtain

$$k^2(x) = (x_t - x)^2 + (x_r - x)^2 + 2(r+x)(r-x) + 2\sqrt{[(x_t - x)^2 + (r+x)(r-x)][(x_r - x)^2 + (r+x)(r-x)]} \tag{49}$$

The x-coordinate is related to the length of the arc s measured from the subreceiver point along any great circle as

$$x = r \cos \frac{s}{r} \tag{50}$$

Taking this relation into Equation 49, we find the value of k along the arc s:

$$k^2(s) = x_t^2 + x_r^2 - 2r(x_t + x_r) \cos \frac{s}{r} + 2r^2 + 2\sqrt{\left(x_t^2 - 2x_t r \cos \frac{s}{r} + r^2\right)\left(x_r^2 - 2x_r r \cos \frac{s}{r} + r^2\right)} \tag{51}$$

The arc length coordinate lines are perpendicular to the iso-range lines and therefore the gradient of $k(s)$ is given by

$$\nabla k = \frac{dk(s)}{ds} = \frac{1}{2k(s)} \frac{dk^2(s)}{ds} \tag{52}$$

Performing the derivation of Equation 51 and substituting the expressions obtained into the equation of the gradient, the following result for the spatial sensitivity of the instrument is finally found:

$$k_s \equiv \frac{1}{\nabla k} = \frac{\sqrt{N(s)}}{D(s)} \tag{53}$$

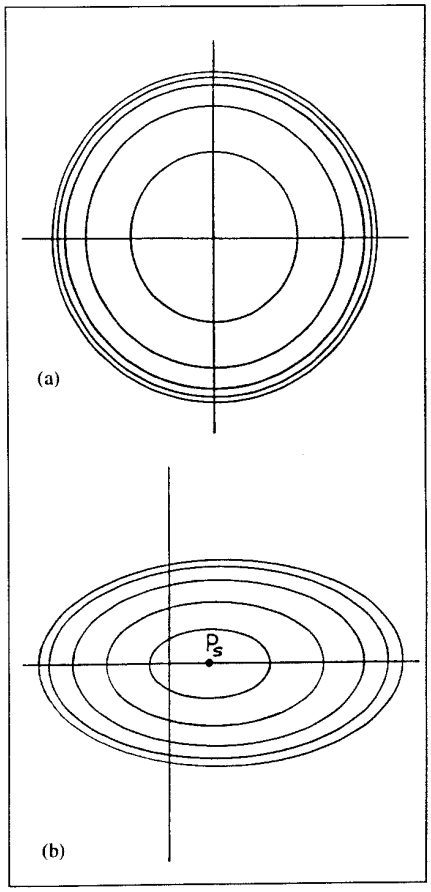

Figure 5. Iso-range lines: (a) transmitter at receiver's zenith; (b) transmitter at arbitrary elevation

with

$$N(s) = x_t^2+x_r^2-2r(x_t+x_r)\cos\frac{s}{r} + 2r^2 + 2\sqrt{\left(x_t^2 - 2x_t r\cos\frac{s}{r} + r^2\right)\left(x_r^2 - 2x_r r\cos\frac{s}{r} + r^2\right)} \quad (54)$$

$$D(s) = \sin\frac{s}{r}\left[(x_t+x_r)+\frac{x_t\left(x_r^2-2x_r r\cos\frac{s}{r}+r^2\right)+x_r\left(x_t^2 - 2x_t r\cos\frac{s}{r}+r^2\right)}{\sqrt{\left(x_t^2-2x_t r\cos\frac{s}{r}+r^2\right)\left(x_r^2-2x_r r\cos\frac{s}{r}+r^2\right)}}\right] \quad (55)$$

The arc length expands from the sub-receiver point to the point of tangency to the Earth's sphere from the receiver point. These limits, which are easy to calculate, are:

$$0 \le s \le \arccos\frac{r}{x_r} \quad (56)$$

The spatial sensitivity of the instrument for different arc lengths has been computed for a spacecraft scenario. The results are shown in the following table, along with the spatial resolution that would be achieved in the case of using the GPS C/A and P codes:

s (km)	$k_s = ds/dk$ (m/m)	ρ_g C/A (m)	ρ_g P (m)
0	∞	∞	∞
10	62	18600	1860
100	6	1800	180
200	3.2	960	96
500	1.4	420	42
800	1.1	330	33
1100	0.9	270	27
3030	0.6	180	18

This table shows that the sensitivity is better for longer distances from receiver to target than for shorter ones. The best sensitivity is obtained at the point of tangency and is about 0.6. Near the sub-receiver point, the sensitivity is very poor as it goes to infinity. For ranges corresponding to arc lengths larger than about 200 km, the sensitivity is better than 3.

When the transmitter is at the zenith of the receiver, the point of specular reflection coincides with the sub-receiver point and we have just seen that the iso-range curves are distributed concentrically around this point, as shown in case (a) of Figure 5. This characteristic of the pattern of the iso-range lines — that they are concentrically distributed around the point of specular reflection — is also valid for the case when the transmitter is not at the zenith of the receiver.

When the transmitter is at other elevation than zenith, the specular point will be somewhere on the Earth's surface between the receiver and the transmitter, as was shown in the section dedicated to the computation of the specular reflection point. In this case, the iso-range lines will also be concentric around the point of specular reflection, and the separation between them will decrease as we go further away from the point of specular reflection. This general result has been depicted in case (b) of Figure 5, where the point of specular reflection P_s appears displaced away from the subsatellite point and towards the transmitter, which is assumed to be located to the right of the figure.

Iso-Doppler lines

First, let us consider the general case as depicted in Figure 6. All three points, transmitter, receiver and target have some velocity with respect to an Earth-centred inertial coordinate system. As the Doppler frequency is proportional to the relative radial velocity, we calculate the relative radial velocities between the three points.

The relative radial velocity for the signal received through the direct path is

$$v_1 = (\vec{v}_r - \vec{v}_t) \bullet \vec{u}_{rt} \tag{57}$$

where

v_1 is the modulus of the radial velocity between transmitter and receiver along the direct path
$\vec{v}_t$ is the velocity vector of the transmitter
$\vec{v}_r$ is the velocity vector of the receiver
$\vec{u}_{rt}$ is the unit vector pointing from receiver to transmitter
and a dot ($\bullet$) denotes scalar product of vectors.

The sign has been chosen so that a positive radial velocity means that transmitter and receiver are approaching each other.

On the other hand, the relative radial velocity involved with the signal received through the reflected path is

$$v_2 = (\vec{v}_r - \vec{v}_p) \bullet \vec{u}_{rp} + (\vec{v}_p - \vec{v}_t) \bullet \vec{u}_{pt} \tag{58}$$

where

v_2 is the modulus of the radial velocity between transmitter and receiver along the reflected path
$\vec{v}_p$ is the velocity vector of the target
$\vec{u}_{rp}$ is the unit vector pointing from receiver to target
$\vec{u}_{pt}$ is the unit vector pointing from target to transmitter.

The difference in radial velocity between the direct and the reflected paths is proportional to the Doppler frequency between the direct and the reflected signals f_D. This difference is given by

$$\lambda f_D = v_2 - v_1 \tag{59}$$

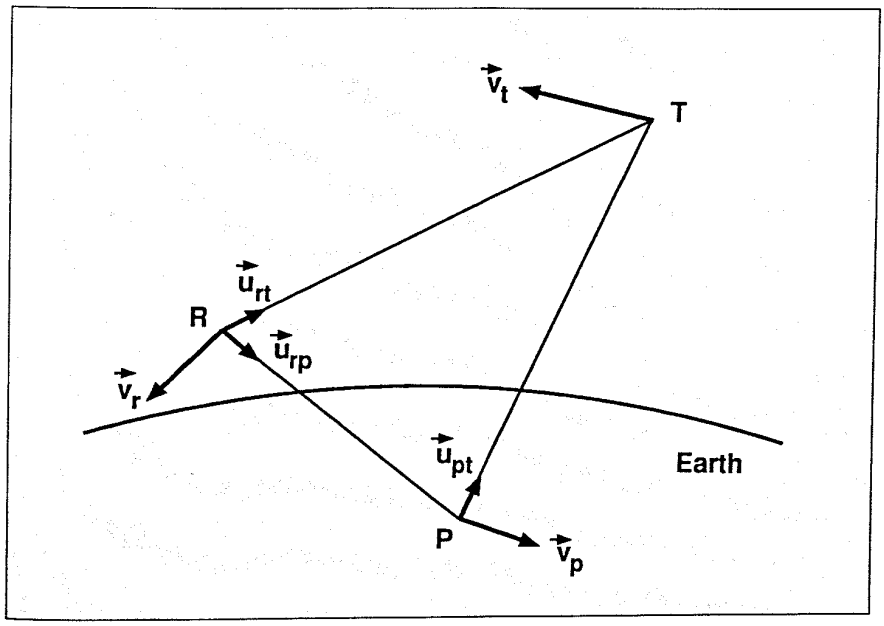

Figure 6. Geometry for the determination of the iso-Doppler lines

Substituting the expressions for v_1 and v_2 into Equation 59, we obtain

$$\lambda f_D = (\vec{v}_r - \vec{v}_p) \bullet \vec{u}_{rp} + (\vec{v}_p - \vec{v}_t) \bullet \vec{u}_{pt} - (\vec{v}_r - \vec{v}_t) \bullet \vec{u}_{rt} \tag{60}$$

Now we introduce the simplification that was anticipated, namely we assume that the distance between receiver and target is much smaller than the distance from either of these two to the transmitter, so that

$$\vec{u}_{rt} \approx \vec{u}_{pt} \tag{61}$$

Introducing this approximation into Equation 60, we find that

$$\lambda f_D = (\vec{v}_r - \vec{v}_p) \bullet \vec{u}_{rp} + (\vec{v}_p - \vec{v}_r) \bullet \vec{u}_{rt} \tag{62}$$

We now look in detail at the right-hand side of Equation 62. The first term is the one found in slant Synthetic Aperture Radar (SAR), except for a factor of 2 due to the monostatic operation of SAR[7,9]. The second term depends on the target point only through its velocity $\vec{v}_p$. As the target velocity is due to the Earth's rotation, which is approximately the same for all points in the footprint, in a first approximation we can consider that this second term is a known constant over the receiver antenna footprint.

If the Earth's rotation speed in neglected, i.e. is $\vec{v}_p = \vec{0}$, then Equation 62 becomes

$$\lambda f_D = \vec{v}_r \bullet \vec{u}_{rp} - \vec{v}_r \bullet \vec{u}_{rt} \tag{63}$$

As the second term on the right-hand side is a constant, which is assumed to be known, the iso-Doppler lines will be contained in the following family of cones:

$$\vec{v}_r \bullet \vec{u}_{rp} = k_D \tag{64}$$

where k_D is a constant given by

$$k_D = \lambda f_D + \vec{v}_r \bullet \vec{u}_{rt} \tag{65}$$

The intersection of these cones and the Earth's sphere gives the iso-Doppler lines. If the Earth's surface is approximated by a plane, the well-known family of hyperbolic lines used in slant SAR is obtained, as shown in Figure 7. Note, however, that although the pattern is the same, the value of the Doppler frequency for each curve will have a constant difference with respect to the usual SAR case.

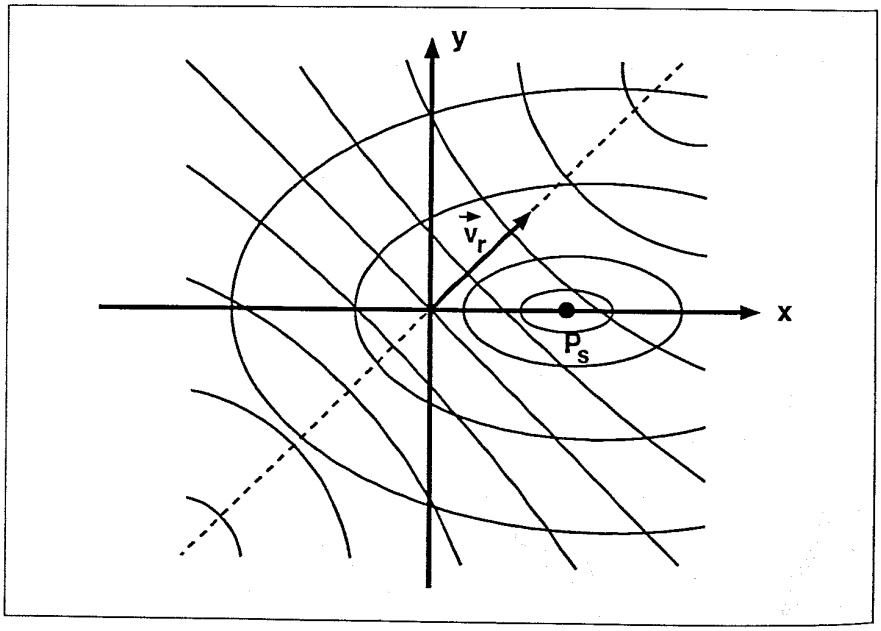

Figure 7. Iso-range and iso-Doppler lines in a bi-state configuration. The iso-range lines form closed contours around the point of specular reflection P_s, which is oriented towards the transmitter location. The iso-Doppler lines are hyperbolas (assuming a far transmitter), oriented in the direction of the velocity of the receiver. Both families of curves are distorted compared to the case of synthetic aperture radar

The conclusion is that, in a first approximation, the pattern of iso-Doppler lines is the same as the usual one found in slant SAR. The small difference stems from the dispersion of radial velocities over the footprint with respect to the transmitter, which is estimated to be in the order of 50 m/s for points 400 km apart.

A further difference with respect to the case of monostatic slant SAR is that the families of iso-range and iso-Doppler curves can be oriented in different directions, depending mainly on the direction of the transmitter and the velocity of the receiver. This is illustrated in Figure 7 where the transmitter is assumed to be located along the x-axis, while the receiver is moving in a direction 45° away from this axis. The iso-range lines appear oriented towards the transmitter, while the iso-Doppler lines are oriented along the direction of motion of the receiver.

3. Signal-to-noise ratio computation

The signal-to-noise ratio (SNR) is computed in two steps:
- SNR for one pulse
- SNR for several pulses.

By 'pulse' we mean one chip of the pseudo-random code which is assumed to be modulating the carrier signal.

3.1. SNR for one pulse

The following multi-static radar equation for distributed targets derived from Reference 9 is applied to compute the SNR in the case in which a single pulse is considered:

$$SNR_0 = \frac{1}{2}\left(\frac{P_t G_t}{4\pi R_1^2}\right)\sigma_b A\left(\frac{1}{4\pi R_2^2}\right)\left(\frac{\lambda^2}{4\pi}G_r\right)\left(\frac{1}{KT_sB}\right) \tag{66}$$

where

SNR_0 is the signal-to-noise ratio, for a single pulse
P_t is the transmitted power (by a GPS satellite, for example)
G_t is the transmitter antenna gain
R_1 is the mean distance from transmitter (GPS satellite) to the receiver antenna footprint on the Earth's surface
σ_b is the mean normalised bistatic radar cross-section across the receiver antenna footprint, evaluated in the directions of transmitter and receiver
A is the area of the receiver antenna footprint on the ground
R_2 is the mean distance from the receiver to the receiver antenna footprint on the Earth's surface
λ is the wavelength of the radiation
G_r is the gain of the receiver antenna
K is Boltzmann's constant
T_s is the system temperature, comprising thermal noise from the scene and receiver noise
B is the signal bandwidth.

The various parameters appearing in Equation 66 are shown in Figure 8.

The system temperature T_s is comprised of the antenna temperature T_a due to the thermal noise received from the observed scene by the receiver antenna, as well as the receiver equivalent temperature T_e due to the noise generated by the receiver itself:

$$T_s = T_a + T_e \tag{67}$$

The receiver equivalent temperature can be expressed in terms of the noise figure of the receiver F as

$$T_e = (F-1)T_0 \tag{68}$$

Figure 8. System geometry used in the computation of the signal-to-noise ratio

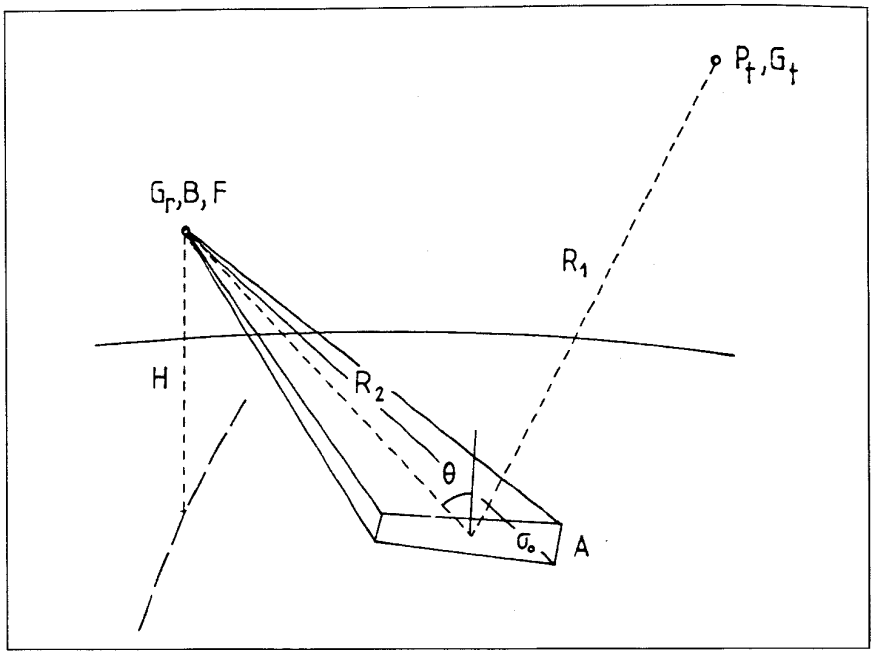

where T_0=290 K is the standard room temperature.

Inserting Equation 68 into Equation 67, we have

$$T_s = T_a + (F-1)T_0 \tag{69}$$

As T_a will generally be lower than about 300 K, and in order to be conservative in the computation of the SNR, we can assume that

$$T_a \approx T_0 \tag{70}$$

and in this case the system temperature appearing in Equation 66 becomes

$$T_s = FT_0 \tag{71}$$

On the other hand, the receiver antenna gain can be related to the illuminated area by

$$G_r = \frac{4\pi R_2^2}{A \cos\theta} \tag{72}$$

θ being the incidence angle.

Substituting Equations 71 and 72 into Equation 66, the signal-to-noise ratio becomes

$$SNR = \left(\frac{S_i/4\cos\theta}{2KT_0B/\lambda^2}\right)\sigma_b\left(\frac{1}{F}\right) \tag{73}$$

where S_i represents the incident power density on the ground

$$S_i = \frac{P_tG_t}{4\pi R_1^2} \tag{74}$$

Looking at Equation 74 in more detail, three contributions can be identified on the right-hand side:

- The first term is recognised as the ratio of the incident power to the thermal noise power per unit area per unit solid angle[7]. This term is governed mainly by the equivalent isotropic radiated power of the transmitter, the distance from transmitter to target, and the bandwidth of the system.

- The second contribution corresponds to the normalised bistatic radar cross-section, averaged over the receiver antenna footprint. It therefore depends on the ocean surface scattering characteristics. A more refined expression for this quantity is shown below.
- The third term represents the contribution of the receiver system, given by its noise figure.

We have to recall however that in the derivation of Equation 74 the brightness temperature of the Earth's surface T_a was assumed to be equal to T_0=290 K. In general, the antenna temperature T_a will be lower than 290 K and a better SNR will result as compared to the one computed in this section.

So far we have not needed either the altitude or the velocity of the platform which carries the receiver for the computations. Thus the result obtained for the SNR in Equation 74 is valid for both spaceborne and airborne receivers.

The rest of this section is dedicated to computing a more detailed expression for the normalised bistatic radar cross-section averaged over the receiver antenna footprint.

As will be explained later, this system is a pulse-limited one in the sense that the portion of ocean surface that contributes to build up the output at a particular time-resolution cell in the instrument is much smaller than the receiver antenna footprint. If a is the pulse-limited footprint, then the normalised bistatic radar cross-section, averaged over the antenna receiver footprint, can be written as

$$\sigma_b = \frac{1}{A} \int_a \sigma_b'(\bar{x}) da \tag{75}$$

where $\sigma_b'(\bar{x})$ is the normalised bistatic radar cross-section of the elemental area da.

In the section dedicated to the description of the measurement of the ocean altimetry, it will be shown that the pulse-limited footprint is very small compared to the target's distance from either the receiver or transmitter. We can therefore neglect the variation in the normalised bistatic radar cross-section due to variations in the target-receiver and target-transmitter directions across the pulse-limited footprint. In other words, the normalised bistatic radar cross-section $\sigma_b'(\bar{x})$ in Equation 75 is constant and can be taken out of the integral

$$\sigma_b = \frac{a}{A} \sigma_b' \tag{76}$$

A theorem of bistatic radar theory states that the normalised bistatic radar cross-section of a target is equal to the normalised monostatic radar cross-section in the bisector direction of the transmitter and receiver directions, when the target is sufficiently smooth[6]. Although the validity of this hypothesis depends in the case of the ocean surface on the sea state, we will assume in the following computations that it holds reasonably well.

Assuming that the theorem of bistatic radar theory can be applied, and because we are dealing with reflections originating from a small area a around the point of specular reflection, we can state that in the normalised bistatic radar cross-section σ_b' is equal to the normalised monostatic radar cross-section σ_0 at an incidence angle of 0°, i.e. in the nadir direction:

$$\sigma_b' = \sigma_0(0) \tag{77}$$

Substituting Equation 77 into Equation 76 we find the expression sought for the normalised bistatic radar cross-section averaged over the receiver antenna footprint, namely

$$\sigma_b = \frac{a}{A} \sigma_0(0) \tag{78}$$

and inserting Equation 78 into Equation 73, the expression for the signal-to-noise ratio corresponding to a single pulse becomes

$$SNR = \left(\frac{S_i/4\pi \cos\theta}{2KT_0B/\lambda^2}\right)\left(\frac{a}{A}\right)\sigma_0(0)\left(\frac{1}{F}\right) \tag{79}$$

3.2. SNR for N pulses

The reflected signal is correlated with the direct signal in order to perform the altimetry measurement. Each correlation is carried out over a time duration spanning N code chips, which we have called 'pulses'. As the correlation process is performed coherently, an improvement by a factor of N is achieved on the single pulse signal-to-noise ratio. Therefore, the signal-to-noise ratio at the output of the N-pulse correlator will be[9]:

$$SNR_N = SNR_0N \tag{80}$$

where SNR_0 is the single pulse signal-to-noise ratio.

Now we shall provide an estimate of the number of pulses N that can be added coherently by computing the coherence time of the signal. The latter is computed taking into account the relative speed between the receiver and the target, but the movement of the ocean surface is neglected as well as the contribution of the speed of the transmitter.

Consider the geometry of the system as shown in Figure 9. The platform is moving at a speed $\vec{v}$ relative to the target, which consists of the pulse-limited footprint a. As will be shown in the section on the altimetry measurement, the pulse-limited footprint has a nearly elliptical shape with its major axis oriented in the receiver to transmitter direction. If we consider the transmitter in the direction perpendicular to the velocity of the receiver as shown in the figure, the Doppler bandwidth B_d of the signal coming from the pulse-limited footprint will be[7,9]

$$B_d = \frac{v\rho_a}{\lambda R_2} \tag{81}$$

where ρ_a is the semi-minor axis of the pulse-limited footprint a, and R_2 is the distance from receiver to target.

Neglecting the contribution to the relative speed of the movement of the ocean surface and the transmitter, the coherence time T_c of the signal will therefore be given by

$$T_c = \frac{1}{2B_d} = \frac{\lambda R_2}{2v\rho_a} \tag{82}$$

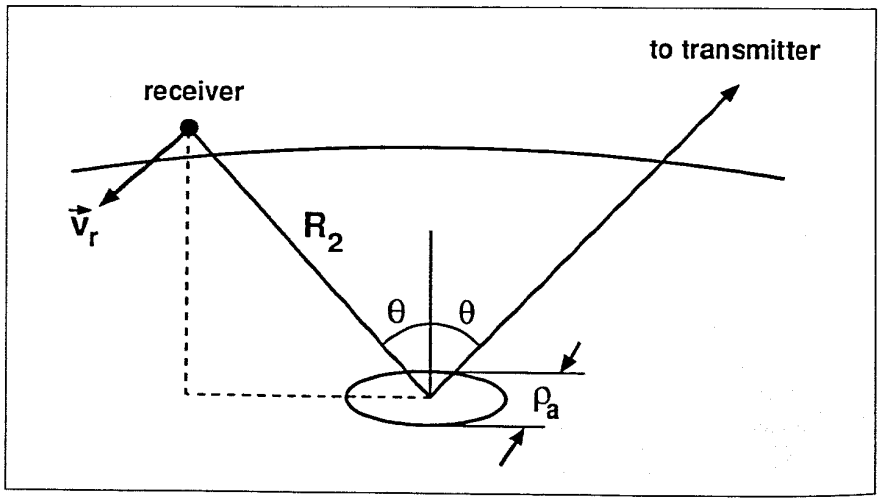

Figure 9. Geometry used in the computation of the Doppler bandwidth and the integration time of the correlators. The width of the pulse-limited footprint is ρ_a, around the point of specular reflection

and the estimated number of pulses that can be coherently added will be

$$N = \frac{BT_c}{2} = \frac{\lambda R_2 B}{4 v \rho_a} \tag{83}$$

3.3. Numerical example: GPS transmitters

The GPS signals are modulated by two pseudo-random codes, the Coarse Acquisition (C/A) code and the Precision (P) code. The chip rate of the C/A code is 1 MHz and that of the P code is 10 MHz. Although the C/A code would lead to a poor altimeter performance, the corresponding signal-to-noise ratio is presented for completeness.

The computation of the signal-to-noise ratio in the case where the receiver is a LEO satellite orbiting at an altitude of 700 km is shown in the table below.

Parameter	C/A	P	Remarks
$P_t G_t$	28 dBW	25 dBW	GPS minimum plus 3 dB
R_1	24×10^6 m	24×10^6 m	
θ	36°	36°	Edge of swath
K	1.38×10^{-23} W/K Hz	1.38×10^{-23} W/K Hz	
T_a	290 K	290 K	
B	2 MHz	20 MHz	RF bandwidth
λ	0.19 m	0.19 m	L1 carrier
F	2 dB	2 dB	
a	27×54 km^2	8.5×17 km^2	GPS elevation >40°
G_r	37 dB	37 dB	4 m ×4 m antenna*
A	43×53 km^2	43×53 km^2	Edge of swath
$\sigma_0(0)$	12 dB	12 dB	ERS-1 altimeter
SNR_0	−9 dB	−32 dB	Single pulse
R_2	913 km	913 km	Edge of swath
ρ_a	27 km	8.5 km	GPS elevation >40°
v	7.5 km/s	7.5 km/s	700 km LEO altitude
T_c	428 μs	1.36 ms	
N	428	13600	
SNR_N	17.3 dB	9.3 dB	N pulse

* If the transmitting power of the GPS system is increased by 5 dB as planned, the size of the receiving antenna could be reduced to 2×2 m^2. If an aircraft is considered, the antenna could be about one order of magnitude smaller due to the longer coherence time.

4. Ocean altimetry measurement

The PARIS concept of using the combination of direct and reflected signals of opportunity to perform ocean altimetry is presented in this section. One of the possible methods for retrieving the height of the ocean over the reference Earth ellipsoid from the received signals is explained and applied for the case in which the transmitters are the GPS satellites.

4.1. Measurement geometry and return waveform

As it was shown in the section dedicated to the iso-lines computation, the locus of constant range points is defined by the intersection of one ellipsoid whose foci are at the transmitter and receiver points and the Earth ellipsoid — in this context the model of the Earth described in the World Geodetic System 84: WGS-84. The WGS-84 ellipsoid and several of the constant range ellipsoids are presented in Figure 10. Taking as reference a particular chip code of the direct path signal, the first echo of

this very same chip code received from a reflection on the ocean surface corresponds to a delay such that the associated constant-range ellipsoid is tangential to the Earth's geoid. This is based on a geometrical property of ellipsoids by which the pair of lines starting from any point on the ellipsoid and passing through its foci form the same angle with respect to the normal to the ellipsoid at that point[5]. This geometrical property could be summarised as follows: at the point of specular reflection, the normal to the Earth's geoid and the normal to the constant-range ellipsoid are the same.

The earliest return of the particular code chip will come from wave crests. As we increase the delay, more reflecting facets will contribute to the signal, up to a point at which the last edge of the code chip reaches the wave troughs[10]. Beyond that point the area illuminated by the code chip remains about the same, and the amplitude will decay due only to either the shaping of the antenna pattern if it is narrow enough, or the decay of the radar cross-section with increasing incidence angle (the theorem of bistatic radar is taken into account here).

The average shape of the resulting waveform will be given by the convolution of the point-target response of the system, the ocean-surface height distribution and the calm-sea impulse response[10]. The antenna footprint will generally be much larger than the pulse-limited footprint.

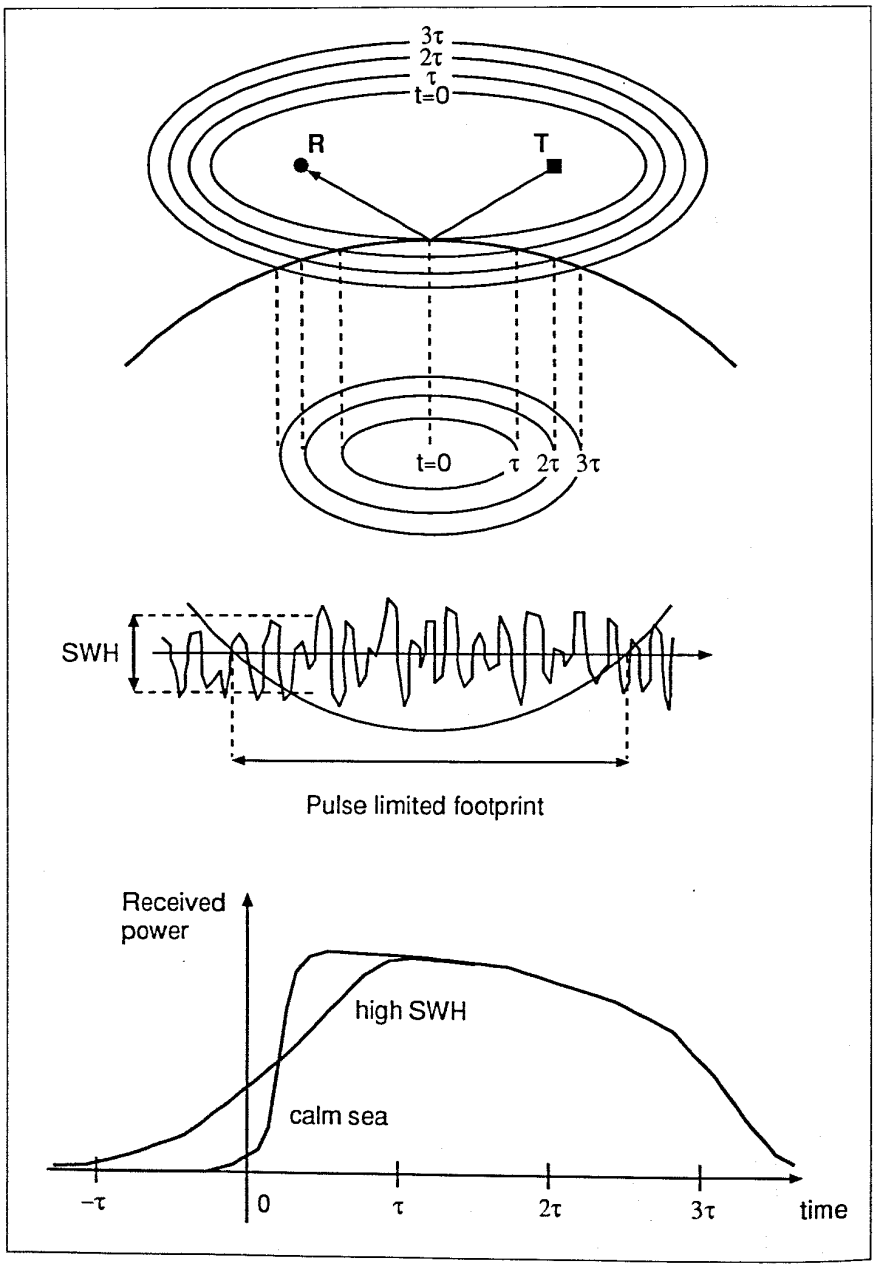

Figure 10. Above: Constant-delay loci, iso-range lines and pulse-limited footprints. Centre: Detail of sea surface: the size of the pulse-limited footprint depends on the Significant Wave Height (SWH). Below: Shape of received power waveform. The model of a nadir-looking echo waveform is assumed. An adequate model for the bi-static case is still required

The illuminated areas for different code chips, as well as the shape of the average received waveform[10], are depicted in Figure 10, where it has been assumed that the model for nadir-looking holds (a proper model for bistatic altimetry is needed). As shown in this figure, the mid point of the rising edge of the received waveform does not depend on the significant-wave-height level, but rather conforms closely to the mean sea level. This point, which is the point of specular reflection, corresponds to a point on the geoid.

The concept for performing ocean altimetry with this system consists of deriving, from the delay measurements, the precise coordinates of the point of specular reflection on the geoid relative to the position of the receiver, in the Earth Centred Earth Fixed coordinate frame defined by the WGS-84 system. The resulting receiver-geoid relative vectors measured as the receiver moves along its orbit will provide a rigid curved line which, once the orbit of the receiver has been accurately determined in the same WGS-84 reference frame, will serve to retrieve the geoid height over the reference WGS-84 Earth ellipsoid. It is also assumed that the receiver's and transmitters' orbits have been precisely measured.

There are basically two error contributions to the determination of the relative coordinates between the receiver and the point of specular reflection on the geoid as illustrated in Figure 11. The first one, case (a) of the figure, is the uncertainty $d\tau$ in the measurement of the delay corresponding to the half-power point of the rising edge of the received waveform. This gives a possible range of values dh along the normal to the Earth ellipsoid and between two constant range ellipsoids, at $+d\tau/2$ and $-d\tau/2$ for the point of specular reflection on the geoid P_s. The second one, presented in case (b) of the same figure, is due to the so-called 'deflection of the vertical'. The deflection of the vertical at a point P_s on the Earth's surface is the angular difference α between the normal to the Earth WGS-84 ellipsoid $\vec{n}$ and the normal to the geoid $\vec{n}'$ at that point. Due to this difference, which is assumed to be unknown, there is an uncertainty ds in the location of the point of specular reflection P_s. However, as we shall demonstrate in the next section, the contribution to the vertical error from the deflection of the vertical is negligible. We recall here that while the geoid is defined as an equipotential surface, the Earth reference ellipsoid is just a geometrical model. In the next section we will examine both sources of error in more detail to assess the performance of the instrument.

The pulse-limited footprint is elliptic in shape, with its largest dimension oriented in the plane of incidence. This dimension has been computed for the case of a receiver aboard a LEO satellite at 700 km altitude, as a function of the elevation of the GPS satellite over the local horizon of the receiver and the code (C/A or P) being used. The arc length from the sub-receiver point to the point of specular reflection is given as a reference. The results are shown in the following table:

GPS elevation (deg)	Arc to specular point (km)	Pulse footprint length (km) C/A	(km) P
0	1551		42
10	1206		32
20	936		25
30	726		20
40	557	54	17
50	418	46	15
60	299	42	13
70	193	39	12
80	95	37	12
90	0	36	11

4.2. Vertical accuracy

In Figure 12, we can locate the point of specular reflection on the geoid by three coordinates: the relative time delay τ between the reflected and the direct signal and

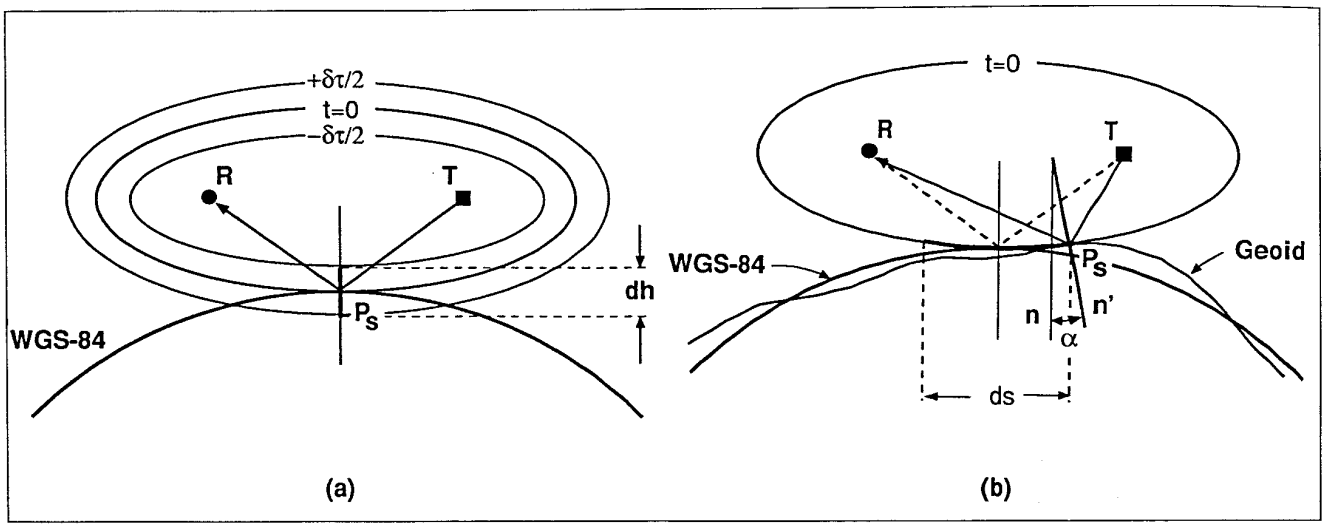

Figure 11. Error contributions to the height accuracy: (a) error in the measurement of the relative time delay of the middle point of the rising edge of the received waveform; (b) deflection of the vertical effect, which is negligible in the vertical direction

the two angles α_1 and α_2 defining the deflection of the vertical. In the figure, only one of the two α angles, the one contained in the plane of incidence, is shown for simplicity. The first coordinate τ is measured by the altimeter and fixes an ellipsoid E in space. The α coordinates are given by the topography of the ocean surface and define one single point on this ellipsoid for which the geoid and the ellipsoid E are tangential (this is the condition for the specular reflection point as was explained in a previous section). Thus, the height h of the geoid over the WGS-84 ellipsoid at the point of specular reflection P_s can be written as a function of τ, α_1 and α_2:

$$h = h(\tau,\alpha_1,\alpha_2) \tag{84}$$

Therefore the vertical accuracy of the altimeter is given by

$$dh = \frac{\partial h}{\partial \tau} d\tau + \frac{\partial h}{\partial \alpha_1} d\alpha_1 + \frac{\partial h}{\partial \alpha_2} d\alpha_2 \tag{85}$$

In the following computations we assume that the altimeter processes the reflected and direct signals such that the delay corresponding to the specular reflection point is measured with a precision given by $d\tau$. The specular reflection point, as already explained, is a point on the geoid, which is the surface of mean sea level, and its associated delay is determined by the half power point of the rising edge of the received waveform. A particular method of combining the direct and reflected signals so as to measure this delay is described in the section dedicated to the system configuration.

The α angles depend directly on the shape of the geoid relative to the WGS-84 ellipsoid. The deflection of the vertical over the ocean is very small, in the order of

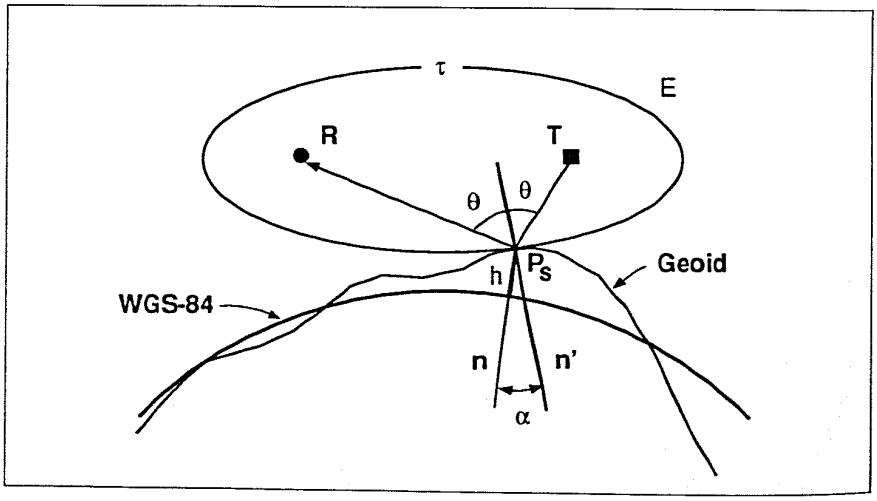

Figure 12. Three coordinates define the point of specular reflection: τ, α_1 and α_2 (α in the figure). Errors in the measurement of these three quantities affect the accuracy of the height measurement

$d\alpha = 10^{-5}$ rad or even less[10,11], and for this reason, we shall see later that its effect on the vertical accuracy can be discarded.

We will now calculate the partial derivatives appearing in Equation 85. For the computation of $\partial h/\partial \tau$, from Figure 13, we can write

$$\frac{\partial h}{\partial \tau} = \frac{-c}{2 \cos \theta} \tag{86}$$

where θ is the incidence angle.

For the computation of $\partial h/\partial \alpha_1$ and $\partial h/\partial \alpha_2$, from Figure 14 we have

$$\frac{\partial h}{\partial \alpha_1} = \frac{2R_2\alpha_1}{\cos \theta} \tag{87}$$

$$\frac{\partial h}{\partial \alpha_2} = 2R_2\alpha_2 \tag{88}$$

where R_2 is the distance from the receiver to the target, as already defined.

Inserting Equations 86–88 into Equation 85, we find for the vertical accuracy

$$dh = \frac{-cd\tau}{2 \cos \theta} + \frac{2R_2\alpha_1^2}{\cos \theta} + 2R_2\alpha_2^2 \tag{89}$$

Because the very small α angles are squared in this expression, their contribution is negligible, and therefore the vertical accuracy can be finally approximated by

$$dh = \frac{-cd\tau}{2 \cos \theta} \tag{90}$$

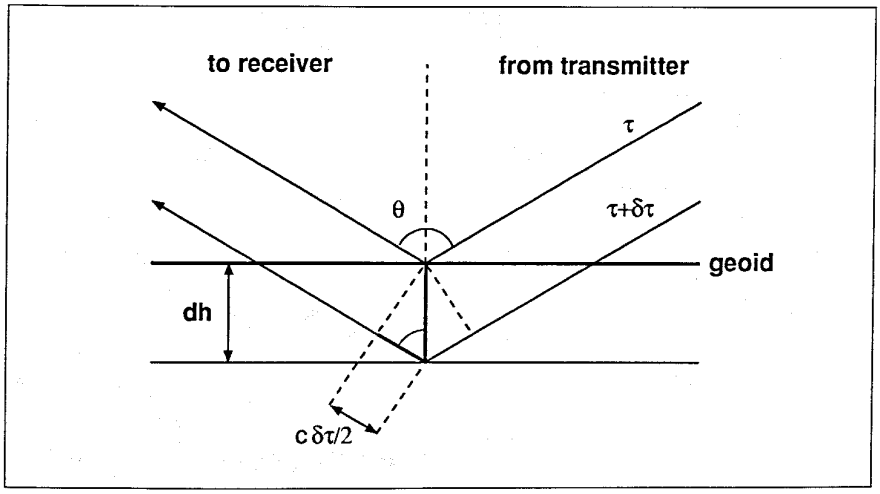

Figure 13. Geometry used for the propagation of delay-time errors into height errors

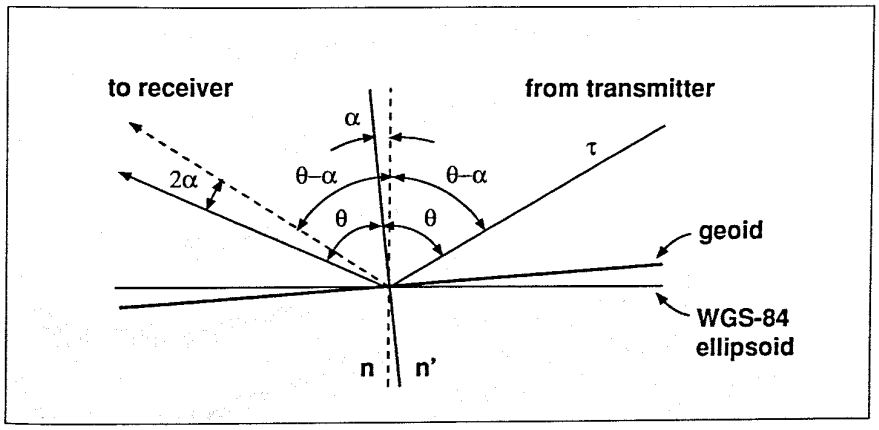

Figure 14. Geometry used for translating the deflection of the vertical into height errors

5. Instrument configuration

Let us assume that there are several transmitters of opportunity whose signals can be used in the way explained in the previous sections. Then for each transmitter above the receiver local horizon, there exists a point of specular reflection on the geoid, as shown in Figure 15. In general, the power available from the opportunity signals is likely to be low, and therefore the down-looking antenna of the altimeter must have enough directivity to achieve the required signal-to-noise ratio. The size of the down-looking antenna is a major issue and depends directly on the power level of the opportunity signal.

The normalised monostatic radar cross-section σ_0 of the ocean for the range of frequencies of interest is large at nadir, but decreases rapidly with increasing incidence angle[7]. The rate of change of the radar cross-section with the incidence angle depends also on the significant wave height and the wind speed. However, as already described, the instrument operates in a pulse-limited mode for which the footprint is so small that variations in radar cross-section with incidence angle can be neglected. Applying the theorem of bistatic radar theory[6], it was shown that the normalised bistatic radar cross-section in the case of specular reflection is the same as the normalised monostatic radar cross-section at nadir. Therefore, as seen in Figure 15, every pulse-limited footprint corresponding to every transmitter will present a large normalised bistatic radar cross-section to the receiver. Depending on the directivity of the receiver antenna, the antenna footprint may enclose only one of the pulse-limited footprints and the beam has to be pointed to each of the other specular points, as depicted in the figure. In this case, the receiver down-looking antenna must be a phased-array capable of steering the beam over a certain area on the ocean surface. This area must be large enough to include the points of specular reflection from a number of transmitters. In the case where the receiver is a LEO satellite at 700 km altitude and the transmitters are the GPS satellites, all specular reflection points generated by GPS satellites at elevations higher than 40° correspond to off-nadir angles smaller than 40°. Therefore, in this example the antenna should be designed to steer the beam within a 40° half-angle cone with its axis parallel to nadir.

The instrument is assumed to be also provided with an up-looking antenna set to receive the direct signals from the transmitters. These signals are used as reference in the processing of the reflected signals and, in fact, they provide the response that would be measured by the down-looking antenna from a point target[8]. For this reason, the processing of the reflected signals is accomplished by correlating them with the direct signal. A block diagram of this type of signal processing is shown in Figure 16, where it is assumed that the transmitted signals are modulated with a pseudo-random code. The signal processor of the instrument is able to compute the expected Doppler frequency of the reflected signal from the positions and velocities of the receiver and the transmitter, which are supposed to be either known or computed. The direct signal is first down-converted and then frequency-shifted

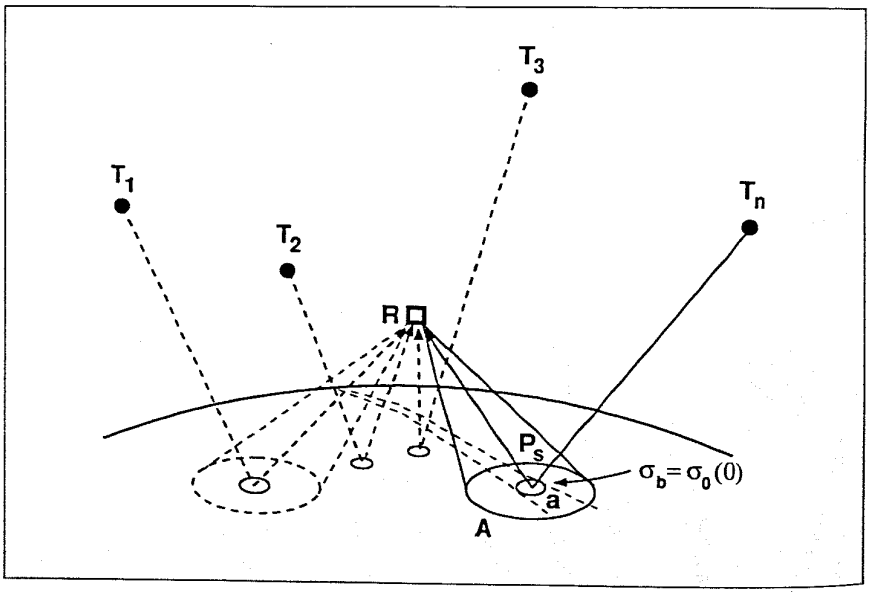

Figure 15. Overall system configuration realising the PARIS concept. Several sources of opportunity generate the same number of reflections. A receiver provided with an upward-looking antenna to receive the direct signal and a downward-looking antenna to collect reflected energy can perform height measurements at the pulse-limited footprints of the reflections. The antenna-limited footprint is larger than the pulse-limited footprint. Depending on the power-link budget, a phased-array antenna may be necessary, to direct the beam sequentially to all reflections. The bi-static radar cross-section at the reflections is close to the monostatic radar cross-section measured at nadir

according to the Doppler shift computed by the processor, in order to match the Doppler frequency of the reflected echo before correlation between the two signals takes place[8]. The signal processor also determines an approximate value of the relative delay between the direct signal and the reflected signal originated at the point of specular reflection.

The direct signal, down-converted and frequency-shifted, is then delayed by this amount except for a number of code chips equal to $n/2$, with n being the number of chips defining the span of delays within which the mean sea level is expected to fall. This frequency-shifted and delayed replica of the direct signal enters a bank of n correlators connected to a tapped delay line of n taps. The second input to the correlators is directly the reflected signal received through the down-looking antenna, after down-conversion. Each correlator correlates a delayed replica of the direct signal with the reflected signal. As there are n correlators connected through n delay taps, the correlation at n different time positions is obtained. The output of each correlator is finally detected to provide a sample of the received power waveform depicted in Figure 10 at a particular time resolution cell. Each of these samples can be interpreted as the amount of power reflected from the ocean surface at a given range relative to the direct signal.

The detected samples will be contaminated by thermal noise and speckle, with speckle being the dominant source of noise if the system has been properly designed with respect to the signal-to-noise ratio. Speckle is caused by the different rate of change of the phase of the components of the reflected signal corresponding to different portions of ocean surface[10]. Assuming a random distribution of the phase of the different components and following the central limit theorem, the amplitude of the output signal of each correlator will have a Gaussian amplitude distribution, and hence the power of the output signal will have a negative exponential distribution. The mean value of the power will therefore be the same as its standard deviation, and time-averaging over a number of samples will be necessary to improve the estimation of the mean power. In order to achieve an accuracy of the level shown in the following table, and according to the following equation giving the standard deviation of the averaged delay $\sigma_{\tau,ave}$ in terms of the sample time resolution $\sigma_\tau = 2/B$ and the number of samples being averaged M_s,

$$\sigma_{\tau,ave} = \frac{\sigma_\tau}{\sqrt{M_s}} = \frac{2}{B\sqrt{M_s}} \tag{91}$$

a minimum of 550 samples would be required, which corresponds in the scenario of LEO and GPS satellites being considered to 0.77 s, ($M_s T_c$) 5.8 km on the ocean surface, or 38% of the pulse-limited footprint.

In Figure 17, typically two main feedback loops would be used, one to fix the power difference between the noise floor and the flat top of the received waveform, and another to maintain the received power waveform at the same location with respect

GPS elevation (deg)	Arc to specular point (km)	Vertical precision (cm)
0	1551	231
10	1206	162
20	936	124
30	726	101
40	557	87
50	418	77
60	299	71
70	193	67
80	95	65
90	0	64

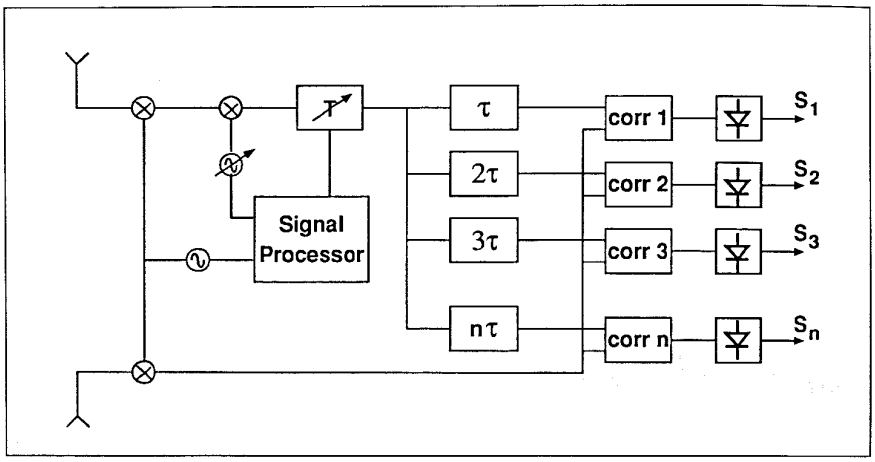

Figure 16. Conceptual block diagram of the instrument: the signal received via the downward-looking antenna is correlated with delayed replicas of the direct-path signal received via the upward-looking antenna. The output of the bank of correlators is detected, forming the samples of the echo waveform. Time averaging is performed at sample level to reduce speckle noise

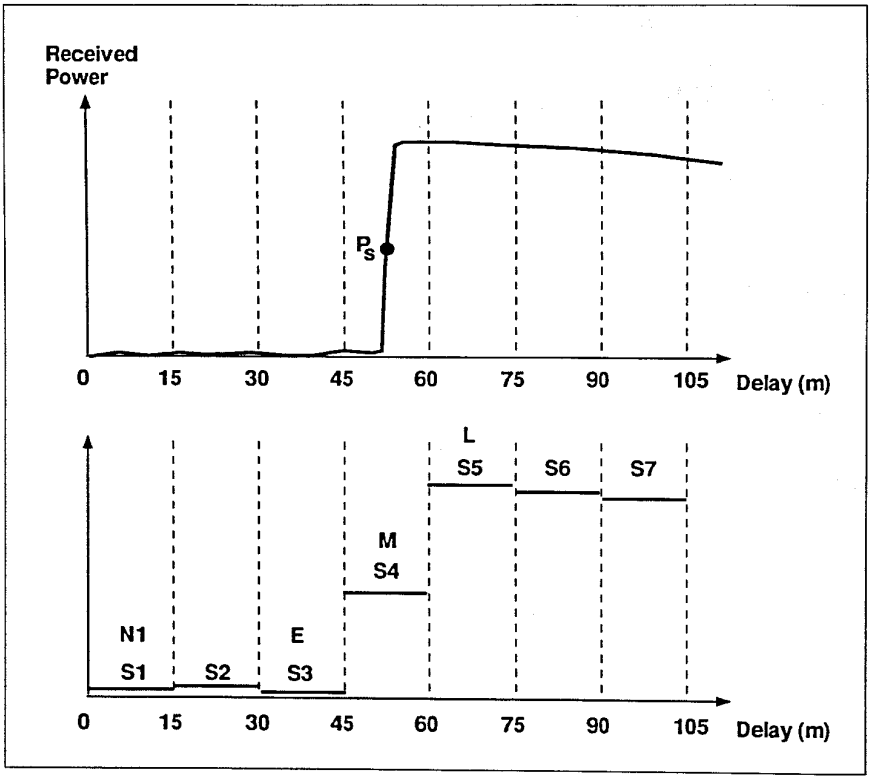

Figure 17. Above: Model for received echo (nadir-looking model assumed). Below: Output of the instrument, for the numerical example of a LEO satellite and the GPS constellation, showing noise, early, middle and late samples used for the signal processing and tracking

to the time-resolution cells[10]. The first loop would be implemented by making use of one sample N_1 on the noisy heading of the waveform and several other samples S_1-S_7 spread symmetrically around the half-power point P_s of the rising edge of the waveform, ranging from the noise floor to the flat top of the waveform. The second loop would be implemented by using an early E, a middle M and a late L sample with respect to the half-power point of the rising edge of the waveform.

In addition to the feedback loops, an altimeter tracker implemented within the signal processor would adjust the delay to be applied to the direct signal before correlating it with the reflected signals so as to have the middle sample with the same power level as the mean power of the signal in the range between the noise and the flat top samples. The delay adjustments would constitute the measurement of the mean sea level, while the precision of the altimeter would be given by the error signal driving the tracker.

An instrument of the kind described would perform the sample averaging onboard, and would deliver to the host platform the power level of all the samples included in one complete waveform, along with telemetry data and in digital form. The number of samples per waveform is basically dependent on the bandwidth of the system, and so is the instrument data rate. In the LEO and GPS satellites scenario, one waveform could consist of 7 samples and the data rate would be about 5 K samples per second

per transmitter. The bandwidth in this scenario is too small to measure the slope of the rising edge of the received waveform properly. However, the concept is valid for measuring this slope provided that the bandwidth of the opportunity signal is sufficient, and therefore measurements of significant wave height and wind speed could also be performed in such a case.

Acknowledgement

The author would like to express his gratitude to the following colleagues: Mr Lopriore for his numerous suggestions and encouragement; Mr Maccoll for help with the power-budget computations; Mr Lucas and Mr Legido for the multipath experiment; Mr Desnos, Mr Petz, Mr Mancini, Mr Silvestrin, Mr Resti, Mr De Gaudenzi, Mrs De Mateo and Mr Ventura for their explanations in their related fields; finally to Mr Feliu and Mr Martin-Rodriguez for the checking of the geometrical relations.

References

1. Rapley C.G. et al. 1990, Executive Summary of the Proceedings of the Consultative Meeting on Imaging Altimeter Requirements and Techniques, June 1990.
2. Alenia Spazio, Feasibility Study for the Constellation of Pulse Limited Nadir Looking Radar Altimeters.
3. Ceva J. et al. 1993, Multipath Interference in Orbiting Receivers due to Earth Surface Reflections, ION GPS.
4. Kurjan D. 1971, Aircraft Altitude Determination Using Multipath Information in an Angle-Measuring Navigation Satellite System, Prepared for NASA by Pennsylvania University.
5. Malaix C. 1940, Tratado de Geometría Analítica', Tomo II.
6. Skolnik M.I. 1980, Introduction to Radar Systems, McGraw-Hill, Tokyo.
7. Ulaby F.T. et al. 1982, Microwave Remote Sensing, Volume 2, Artech House, Norwood, USA.
8. Bernfeld M. et al. 1965, Matched Filtering, Pulse Compression and Waveform Design, Technical Session, January 1965.
9. Curlander J.C. et al., Synthetic Aperture Radar: Systems and Signal Processing, J. Wiley & Sons, New York.
10. Marth P.C. et al. 1993, Prelaunch Performance of the NASA Altimeter for the TOPEX/POSEIDON Project, *IEEE Trans. on Geoscience and Remote Sensing*, Vol. 31, No. 2, pp. 315–332.
11. CNES 1993, Brochure on TOPEX/POSEIDON Measurement Results.

Manuscript received 18 November 1993